AIAA SciTech Forum
6-10 January 2025, Orlando, FL
AIAA SCITECH 2025 Forum

10.2514/6.2025-1250

Modeling of the A320 Landing Gear Drag During Their Extension and Retraction

Christoph Deiler*, Nicolas Fezans†
DLR (German Aerospace Center), Braunschweig, 38108, Germany

The modeling of the transient drag increase during the extension or retraction of landing gears does not seem to have been studied in details. The aerodynamics and aeroacoustics of fixed and retractable landing gears have been investigated by various groups with the aim to the reduce their drag, especially for fixed landing gears, or their noise. For aircraft designers, there is almost no need for investigating the comparatively short duration (about 20 s) of the gear extension or retraction, which explains the lack of publications on this topic. For non-retractable landing gears, the contribution to the overall aircraft drag is often minimized by covering most of the gear leg and wheel with a fairing. In terms of drag models, this contribution is often not distinguished from the overall aircraft drag. For retractable landing gears, the contribution of the landing gear to the total drag can be determined experimentally by using system identification techniques to identify two separate models: one with the landing gear extended and one with the landing gear retracted, and by subtracting the obtained drag values. The experimental determination of the transient evolution of the drag during the transition between these two positions is difficult and only useful for very specific use-cases. For instance, for making very precise predictions of the deceleration of an airliner in final approach with low power, knowing the actual time evolution of the drag within the 15–20 seconds of the gear extension can improve the predicted airspeed at the end of the extension by about 1–3 knots. Leveraging a series of prior work by the authors on flight performance identification for the Airbus A320ceo and A320neo aircraft and a dataset of operational flights with A320neo, a methodology allowing the identification of the transient drag during the landing gear extension is proposed and demonstrated. Data from 804 gear extensions from three A320neo aircraft during regular operations were used for this work. The causes for the highly nonlinear evolution of the drag during the gear extension are explained. A simple model of the landing gear drag as a function of the gear legs and doors positions is derived. This model is valid for the A320neo and all other models of the A320 family which shares the same gear. Similar effects as those identified for A320 can certainly be expected for many airliners, as they often have similar landing gear kinematics and geometries as the A320.

I. Introduction

The quality of flight dynamics models is, among many other components, crucial for the representativeness of flight simulators such as the ones used for training professional pilots. Various levels of representativeness for simulation-based training devices were defined by ICAO and are used by most local aviation authorities and used for qualifying simulators worldwide. In Europe, this served as a basis for the JAA (Joint Aviation Authority) specifications for Flight Simulation Training Devices (FSTD), which now turned into the EASA CS-FSTD since 2012 [1]. For the so-called Full Flight Simulator (FFS) devices, four levels named A, B, C, and D are defined and the level at which a simulator is certified determines which type of training can be performed (and recognized for the qualification of pilots) with this simulator. FFS Level D is the highest level and simulators certified at this level can fully replace in-flight training, for all kinds of training content. The quality of the flight dynamics model used for level D simulators is precisely defined, based on standardized maneuvers and tolerance bands for the main flight parameters during the aircraft reaction.

Developing and validating a model to level D requirements across all the flight envelope and for all configurations (high-lift, landing gear, spoilers/speedbrake) and thrust settings is a time-consuming and costly process. Numerous

*Scientific Advisor, Institute of Flight Systems, Lilienthalplatz 7, Braunschweig, 38108, Germany, AIAA Senior Member
†Scientific Advisor, Institute of Flight Systems, Lilienthalplatz 7, Braunschweig, 38108, Germany, AIAA Senior Member

researchers are working on means to improve the generation of such models, for instance by optimizing the planning of the flight tests during which flight data are recorded. This can include optimizing the flight planning to optimize the ratio between flight time spent performing system identification and Qualification Test Guide (QTG) maneuvers to total flight time. By performing richer/more complex maneuvers, for instance using multi-axis maneuvers [2–5], better models can be derived from less data.

Recently, the authors designed multi-step methodologies to improve the quality of the flight performance of existing flight dynamics models leveraging large amount of operational data (flight data recorded during regular flights in airline operations) [6]. The aim of these prior works was not only to reach level-D quality on the flight performance aspect, but to go even beyond level-D to improve the quality of the optimized configuration changes made by the DLR "Low Noise Augmentation System" (LNAS) [7–9]. This system uses high-quality performance models of the aircraft and information on the current state of the aircraft and the current wind conditions to help pilots in flying efficient and more silent approaches by optimizing the timing of the speed, high-lift, and gear configuration changes. The methodology proposed in this work to identify the transient changes of the drag during the landing gear extension relies on aircraft performance models (including engines models) with fixed configurations (high-lift, trim, spoilers/speedbrakes). Each configuration is modeled through separate parameters. The aerodynamic characteristics during transitions between these discrete configurations are obtained by linearly interpolating based on the measured deflection angles. On modern aircraft, the exact slat/flaps and spoiler deflection angles are usually measured and known by the flight control system(s). Additionally, the modeled effects evolve fairly linearly between two modeled values, such that the errors induced by interpolating linearly can be neglected.

The situation is different for the landing gears. During opening/closing of the landing gear doors and during extension/retraction of the gear legs, their exact positions are usually not known: only the final positions are detected by means of specific sensors. One sensor detects that the landing gear is locked in retracted position, and another one that it is locked in extended position. Similarly, sensors detect that the landing gear door is fully opened or closed. The gear extension and retraction sequences are well defined and can, for most aircraft, be summarized as follows: a) the door opens, b) after confirmation that the door is fully opened (based on the corresponding sensor) the gear extends, c) when the gear is confirmed locked in the extended position, potentially the door or a part of it closes again. The reverse sequence is used for retraction, with adapted confirmation steps (e.g., confirmation of the locked the gear in the retracted position instead of the extended position). The duration and speed of each of these individual motions can easily be modeled and simulated. The relationship between a given door and gear position and their impact on the aerodynamics of the aircraft is highly nonlinear and not easy to determine through CFD due to massive local flow separation and unsteady wake. For pure performance modeling (e.g., modeling drag), the expected benefit is usually not worth the enormous costs of such computations. Most CFD work in relation with extended landing gear configurations is linked to aeroacoustics considerations. Such studies focus on determining or reducing the noise generated by the landing gear (see for instance [10] and [11, Sect. 1.1]) possibly in combination with the landing gear bay cavity and the landing gear doors. For instance, in [12, 13] various measures to reduce the noise emitted by the gear while considering the gear bay open cavity are investigated. Various ideas to influence the noise generated by the gear bay are also investigated, as for instance in [14] where sawtooth-shaped chevrons are placed at the front of the bay opening. In these aeroacoustic investigations, the landing gear drag is often secondary but could potentially be an interesting side product for flight performance models. Considering the drag evolution during gear extension/retraction would however not be worth the additional effort (CFD mesh-adaption or additional mechanics for the wind tunnel model).

This paper presents a method to identify the nonlinear evolution of the drag during the landing gear transition from a large amount of operational flight data. The method is demonstrated using Airbus A320neo operational data and the causes for the identified highly nonlinear drag evolution during the transition are explained. It seems that the exact drag evolution during extension and retraction of the landing gears has not been considered in prior (published) work. In practice, implementing the pitching moment reaction and the overall final drag increase are probably enough to fulfill the requirements of the EASA CS-FSTD [1]. As the gear extension and retraction are almost always taking place in a relatively changing flight conditions (accelerating, descending, changing engine thrust level, capturing the glide slope), the operational data usually contain some other simultaneous maneuvers which makes the extraction of only the gear contribution challenging. In the present work, this problem is solved by putting some significant effort to subtract as much as possible the other effects by using well-calibrated performance models and by using a many as 804 gear extension maneuvers.

The evaluation is divided into three parts: data preprocessing, aerodynamics analysis, and model identification. In Fig. 1 these three parts are further divided in different steps. The basic flight data processing is already available from previous work on flight performance model determination [6, 15, 16] and is not covered in this paper, but required

for the data evaluation. The first data preprocessing step consists in extracting the gear extension maneuvers and data from the complete flight data sets. The data is then synchronized for the further analysis. The aerodynamics analysis consists of the aerodynamics coefficient calculation for the current flight conditions (speed, altitude, angle of attack etc.) using the performance model (including thrust model) obtained with the method already published in [6] for the gear up configuration.

The difference between the drag coefficient calculated from the recorded flight data and the drag coefficient predicted by the model in gear up configuration provides an estimate of the drag coefficient variation due to the landing gear and the gear doors for each gear extension maneuver. The obtained time series for the gear/doors-induced drag coefficient are fairly noisy, but by averaging a significant number of them a relatively clean and smooth averaged time series. To match this time-evolution a semi-empirical gear drag model structure is defined. It is partly based on the analysis of the extension sequence obtained from a video recorded during maintenance operations and on which the gear extension of the DLR A320 ATRA test aircraft can be seen (aircraft jacked up on ground) as well as flight mechanical judgment of how the different steps and phases of the motions need to be parameterized to allow reaching a good agreement with the experimental data. Finally, the parameters of this model are identified from the available data.

The paper is structured as follows:

- a description of the landing gear extraction of the Airbus A320 is given in section II;
- section III describes the operational flight data used;
- the way the landing gear drag is extracted from the flight data is described in section IV;
- section V presents the proposed gear model, and finally
- section VI presents the results obtained.

A summary and outlook are given in section VII.

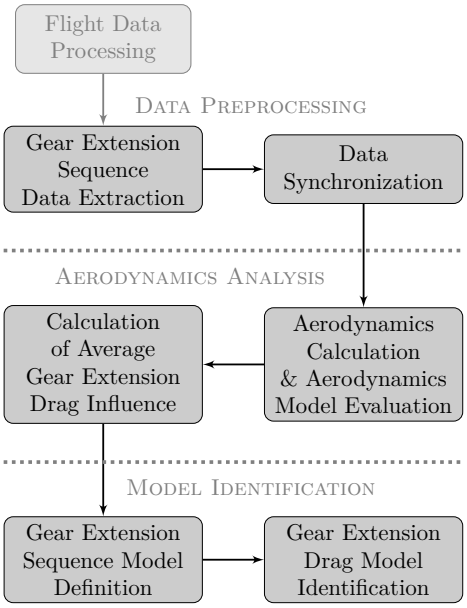

Fig. 1 Data evaluation scheme for gear extension drag model identification from operational flight data

II. Landing Gear Extraction of the Airbus A320

For this work, operational flight data from Airbus A320 aircraft are available. Although the data was gathered with A320neo ("new engine option") aircraft, the landing gear extraction is similar to the ceo ("current engine option") version, such as the DLR Airbus A320 ATRA ("Advanced Technology Research Aircraft") research platform. Hence, some relevant information about the landing gear extension sequence of the A320 can be also obtained from ATRA, for which pictures of the landing gear and video footage of its extension are available. Figure 2 shows two pictures of the aircraft in side and front view with gear extracted during landing and on ground.

(a) Side view during landing **(b) Front view on ground**

Fig. 2 DLR Airbus A320 ATRA Landing Gears (for both pictures, credits DLR (CC BY-NC-ND 3.0))

Fig. 3 Full frame from DLR's Airbus A320 ATRA maintenance video with red rectangles indicating the areas of interest for the gear extension sequence analysis, cf. Figs. 4 to 5.

In the following, the gear extension sequence is detailed and the timing of the different sub-steps is provided. This timing was extracted from a video taken during the aircraft maintenance with the Airbus A320 ATRA jacked up in the hangar. During this maintenance-related test, the hydraulics system was not powered by the usual aircraft systems, but supplied by an external ground power unit. The aircraft was not moving and therefore not experiencing load factor variations, which could influence the apparent/inertial forces acting on the gears. Whether these differences would yield significant differences or uncertainties was unclear at first. The good agreement found between the timing of the main events in the maintenance video and the drag variations observed on the available flight data suggests that both situations were sufficiently comparable for the purpose of this model development.

The timelines of the main events during the extension sequences of nose and main gears are given in the following. Unfortunately, the available video does not contain the complete sequences from the begin of the door opening but starts with doors already moving. Hence, the time stamps of the events are defined with respect to the time when the nose gear doors reach their fully open position. The sequences for both gears (nose and main) are extracted from the same video: the images shown later are zoomed in to the interesting part of the video frames. For orientation, Fig. 3 shows one full frame where the two areas of interest for the nose gear and the main gear are highlighted with red rectangles.

Fig. 4 shows a sequence of the main events during the nose gear extension, with the corresponding timing* and cropped video frame. The start of the nose gear motion after 1.37 s can be seen by the aft nose gear doors (which are split into two parts) slightly opening and then resting between 1.61 s and 1.77 s, being then further opened when the nose gear is extending. These aft parts of the nose gear doors remain open with the gear extended and the front doors are closed again at the end of the sequence between 14.87 s and 16.27 s.

Fig. 5 shows the equivalent sequence of the main events for the main gear extension. Left and right main gears are assumed to move symmetrically and only the right gear is shown here, which is easier to see due to the camera position aft of the right wing. After the main gear doors are fully opened, the first indication of the motion of the gear leg is the slot starting to appear at 1.34 s between the gear leg cover, constituting a portion of the wing lower surface when the gear is retracted, and the remaining part of the lower wing surface. Similar to the nose gear there is a short rest and the gear starts moving constantly at 1.87 s, extracting the wheels out of the aircraft fuselage (5.47 s) with full extension about 9 s later. The main gear doors are closing again at 14.87 s, closing the wheel storage bay inside the fuselage belly while the main gear leg storage in the lower side of the wing remains open when the main gear is extended.

Note that the short resting of the main and nose gears at the beginning of the motion (difficult to assess from the steady pictures) could originate from a delay between the unlocking of the gear, potentially resulting in a motion caused by the gravity force, and the time at which the hydraulic actuators start to operate. However, this will not significantly affect the drag influence and hence the work presented in this paper. As it lasts less than 0.3 s, it will be neglected later in the proposed drag evolution model.

*remember that here $t = 0\,s$ corresponds to front nose gear doors reaching their fully open position

Fig. 4 Key frames for the nose gear extension motion extracted from the Airbus A320 ATRA maintenance video; credits DLR (CC BY-NC-ND 3.0)

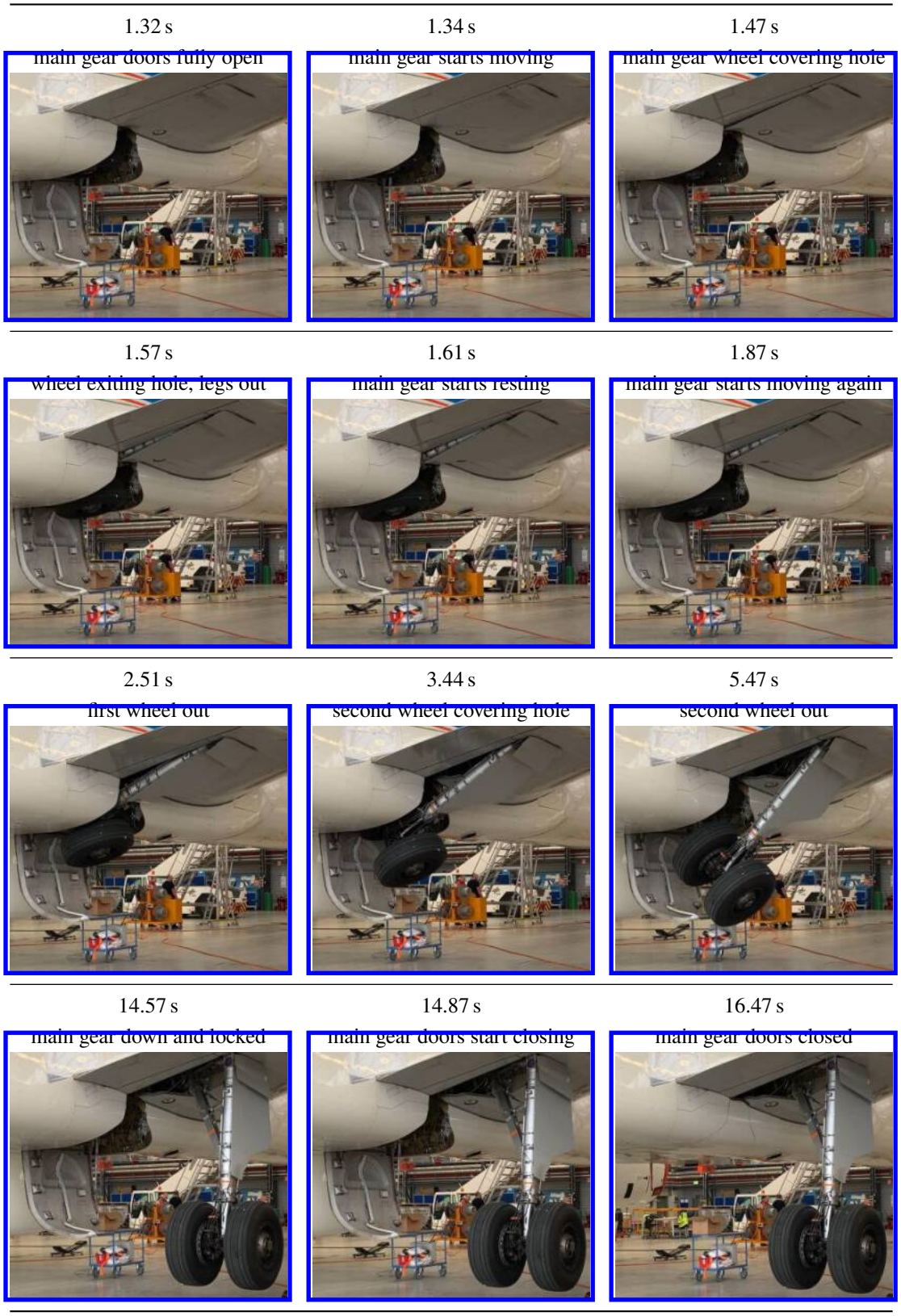

Fig. 5 Key frames for the main gear extension motion extracted from the Airbus A320 ATRA maintenance video; credits DLR (CC BY-NC-ND 3.0)

III. Operational Flight Data and Preprocessing

A. Available Operational Flight Data Recordings

This work is based on flight data recorded during operational flights by an application running on the pilots' electronic flight bags (EFBs). This application was developed by DLR and installed on the EFB's of numerous Airbus A320neo aircraft of a major European airline in preparation of the SESAR Very Large Demonstration (VLD2) ALBATROSS project[†]. The recorder is able to record messages sent via ARINC 429, ARINC 834 or ARINC 717 using different interfaces depending on the EFBs it is installed on.

To quickly reduce the amount of data to process, the portions of the flight with true airspeed lower than 130 kts or height below either 50 ft AGL or 500 ft MSL are excluded to ensure that no data in ground effect were considered. These limits do no restrict the evaluations, but allow avoiding any special conditions of flight near ground during landing and engine power reduction. The range covered by the considered flight data after the first down-selection is given in Table 1. In this table, the number of data points only includes the data which was used for the evaluation. Figure 6 visualizes the distribution of available flight data on an altitude-Mach plane in the form of the convex hulls of the envelope covered, with separate convex hulls for the different aircraft flap/slat configurations.

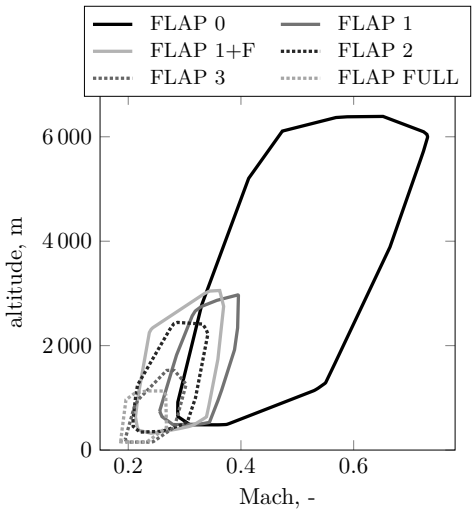

Fig. 6 Convex hulls of the covered flight envelope: one altitude-Mach hull for each flap/slat configuration.

Table 1 Overview of the dataset used.

number of aircraft		3
number of flights		844
data envelope	**min**	**max**
barometric altitude	500 ft	20 964 ft
Mach number	0.1866	0.7311
total weight	48.57 t	73.44 t

Following the first down-selection, the set of flight data used is further reduced. The relevant information is extracted and further processed. Initially, the data were recorded directly from aircraft avionics with no modification. Then they were decoded and re-sampled to obtain a series of individual data channels with a sampling rate of 50 Hz. This corresponds to the in-house standard processing step for an aircraft system identification task. For the work presented, the sample rate of 50 Hz might appear unnecessarily high because the focus lies on the aircraft flight performance and not on the identification of the aircraft dynamic behavior. However, some of the following calculations require transformations of, e.g., accelerations, so using a 50 Hz sample rate directly instead of reducing the data size further by using a lower sampling rate prevents generating avoidable artifacts in the subsequent processing steps. The re-sampled data contains the following channels:

- time stamp (UTC/Zulu time in seconds);
- body-fixed accelerations: longitudinal, lateral, vertical;
- body-fixed angular rates: pitch, yaw, roll;
- inflow/atmosphere: corrected angle of attack, estimated angle of sideslip, true airspeed, Mach number, static temperature;
- altitude: barometric, barometric corrected, GPS, radio height;

[†]ALBATROSS, the most energy-efficient flying bird; this project has received funding from the SESAR Joint Undertaking under the European Union's Horizon 2020 research and innovation programme under grant agreement No 101017678.

- engine fan speed (both engines);
- aircraft gross weight, longitudinal CG position;
- configuration: landing gear status (main left/right and nose: several binary sensor readings indicating commands, specific positions, and locked/unlocked status), flap position, slat position;
- control inputs: spoiler deflection (left/right, spoilers 2 to 5), horizontal stabilizer deflection;
- anti-ice system status: wing, engine.

The flight data is adequately processed for aerodynamics evaluation and model determination. All data are converted to SI units and, whenever necessary, channels are corrected to comply with standard flight mechanics reference frames (cf. [17, 18] and similar national standards). For example, accelerations are transferred from the position of their measurement to center-of-gravity for further evaluation and aerodynamic coefficient calculation.

B. Flight Data Preprocessing

1. Extraction of the Data Corresponding to the Gear Extension Sequence

The available set of operational flight data is first searched for the gear extension sequences based on the gear status flags and the gear lever position selected by the pilots. For each gear extension maneuver found, a short time segment is extracted. The gear extension sequence is defined for the purpose of the paper starting with the gear down command by the pilot (gear lever selection) and ending with the gear doors closed again after the gear is down and locked. More specifically, the flight data are automatically searched for a change of the following landing gear-related signals, i.e.:

- main landing gear compressed,
- left hand gear not locked up,
- left hand main landing gear status [retracted/extended],
- right hand main landing gear status [retracted/extended],
- nose gear status [retracted/extended].

Data segments during which the gears are moving are automatically detected and extracted with some margins of several seconds before the gear extension is starting and after the sequence (including doors closing again) has ended. Figure 7 shows an example of extracted time segment in which a gear extension during approach was detected. The first two plots show the flight condition (altitude and true airspeed). The third plot shows the drag coefficient, relevant for this work, derived/calculated from the flight data[‡]. Finally, the last three plots show the gear status flags/sensors. The difference between both drag coefficient curves is the base for the subsequent modeling approach. Looking at the time histories already reveals the gear drag influence over time, which is nonlinear during the extension. The main part of the drag increase visibly occurs in the relatively short time between 12 s and 16 s.

Out of the 844 available recordings, 804 gear extension maneuvers have been extracted for which the data were complete and appear consistent (e.g., no spikes or dropouts) during the extension and which were found valid for the further evaluation. The landing gear was mainly extended while the aircraft was in FLAP 2 configuration. Due to (presumably) operational reasons, the gear was also extended in about 5% of the cases during other parts of the approach with other high-lift system configurations. To prevent unwanted effects from inducing additional error in the analysis, only gear extension maneuvers for which the high-lift configuration remained constant are considered. An overview of the number of gear extensions found and validated for each of the high lift system configurations is given in Table 2. All of them are considered for the next analysis steps.

Table 2 Distribution of the extracted gear extension maneuvers over the high lift system configurations

high lift configuration	number of time segments
FLAP 1	13
FLAP 2	761
FLAP 3	29
FLAP FULL	1

[‡]The scale on the vertical axis of this specific plot are left out for confidentiality reasons and to not reveal the aircraft's flight performance.

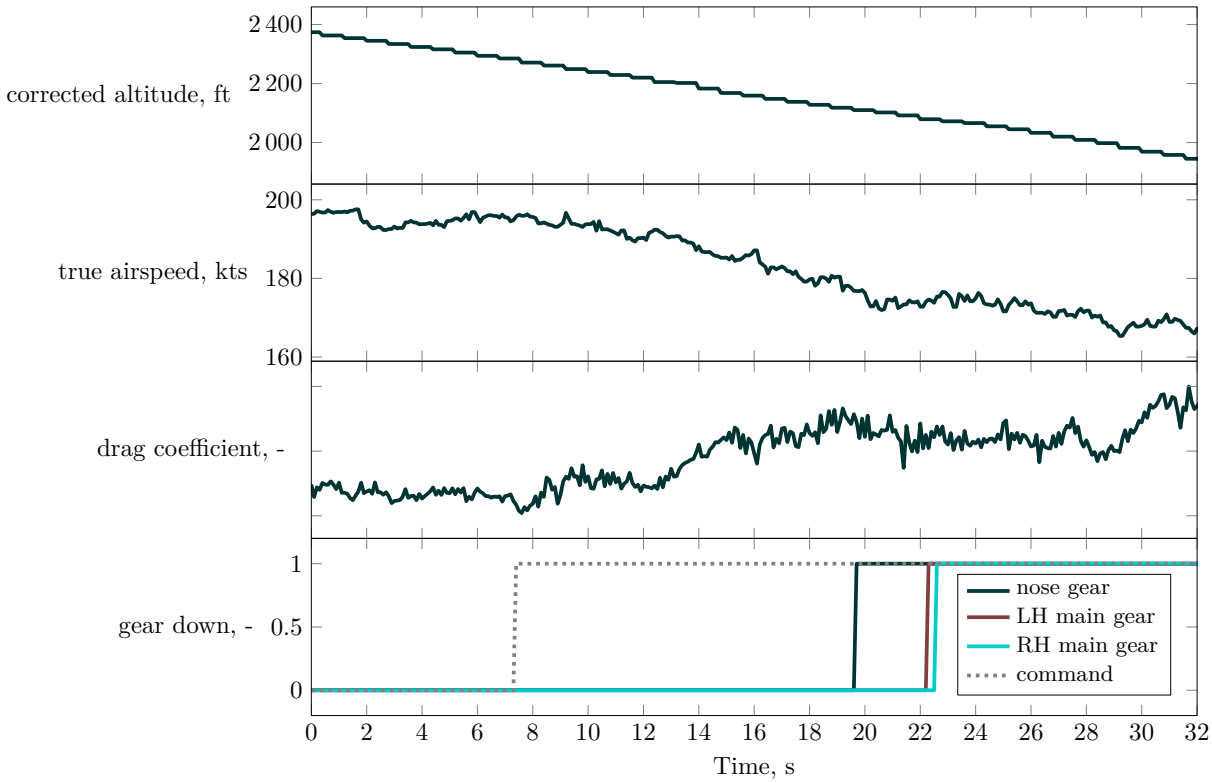

Fig. 7 Example of a gear extension segment during final approach: flight condition (two top plots, altitude and true airspeed), drag coefficient calculated from measurements, and available gear flags from the flight data records (bottom plot).

2. Synchronization of the Time Segments

Each of the extracted time segments contains a gear extension maneuver, and these have to be synchronized to a common time reference, e.g., the gear down command. The gear extension duration is assumed to be similar for different aircraft tail numbers, different flight and varying conditions (see for instance the change in altitude and speed in Fig. 7), and sometimes different aircraft high-lift configurations. In practice, slightly different behaviors could result from differences in hydraulic pressure or vertical load factor during the extension, which could induce inaccuracies in the time synchronization. The data recording system itself can also cause significant time synchronization issues. Some signals related to the aircraft gear are available are recorded with a very low sampling rate. When such a signal changes from 0 to 1 from one sample to the next, the exact moment at which it really happened could have been any time between these two samples. This can happen for signals indicating the start of the maneuver (e.g., the gear down cockpit command signal) but also for signals indicating intermediate steps or one of the final ones (e.g., gear locked down). The true final state of the sequence (i.e., gear doors closed) is not available in the recorded data. With uncertainties at the beginning and the end of the interval, the uncertainty on the duration is even larger.

When looking very closely at the data, slight variations in the duration of the sequence and its substeps seem to be present but are small compared to the overall sequence duration. With the limited sensors available, it does not appear possible to determine the exact causes for these variations, nor does it appear significant enough to justify investigating this further (at this stage). Eventually, through the averaging of many such gear extension maneuvers, a nominal (or average) gear extension sequence and duration is identified. Especially the uncertainties induced by the low sampling rate should compensate each other well, on average.

IV. Extraction of the Gear-Induced Drag During Extension

By means of a baseline flight performance model of the aircraft with retracted gear, the drag caused by the landing gear can be extracted from flight data. This section describes the exact steps of this process.

A. Basic Idea

The underpinning idea for the extraction of the landing gear drag $C_{D,\mathrm{LG}}$ is to consider that it corresponds to the difference between the apparent, or measured, drag coefficient $C_{D,\mathrm{meas}}$ and the drag coefficient $C_{D,\text{model w/o gear}}$ that is predicted by a well-calibrated drag model of the aircraft with retracted gear. Note that the drag model cannot be perfect, so a generic term representing the (unknown) model error e_{C_D} is needed to properly define $C_{D,\mathrm{LG}}$.

$$C_{D,\mathrm{LG}} = C_{D,\mathrm{meas}} - C_{D,\text{model w/o gear}} + e_{C_D} \ . \tag{1}$$

The determination of the drag coefficient $C_{D,\mathrm{meas}}$ from the measurements is described in section IV.B and the aerodynamic model used to determine $C_{D,\text{model w/o gear}}$ is described in section IV.C. For these two steps (subtracting thrust and non-gear-related aerodynamics), very good performance models are required and were available through prior work by the authors [6, 15, 16]. Each of the gear extension maneuvers is performed at different and varying conditions (speed, altitude, temperature, etc.) and these conditions are also not constant during the maneuver. So, if the performance model used lacks accuracy, it cannot be simply corrected afterwards by identifying some constant bias for each time segment: the model should be well calibrated beforehand. The different sources of error are detailed later in Eq. (18) but simply represented by the e_{C_D} term in Eq. (1).

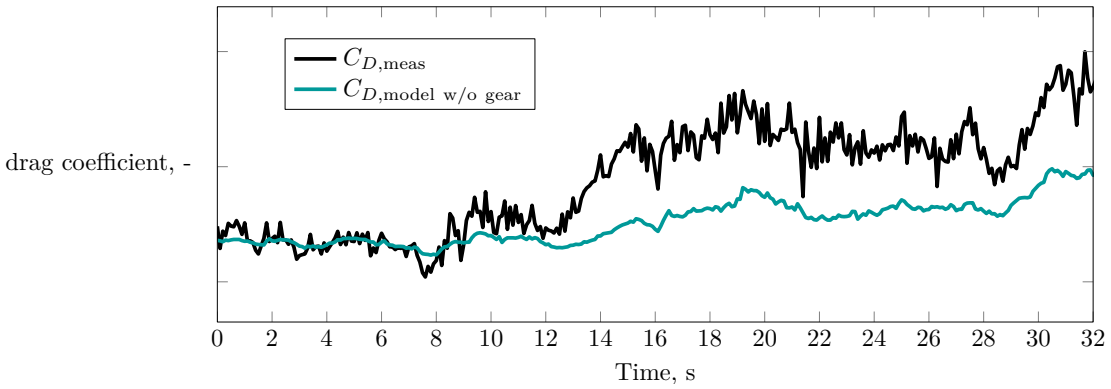

Fig. 8 Example of extracted gear extension segment during final approach: drag coefficient calculated from measurements (black) and from simulation without gear influence (persian green); see also Fig. 7.

B. Aerodynamics Coefficients From Flight Data

The measured flight data allows directly calculating the (translational) aerodynamic coefficients using the predicted engine thrust as given e.g., in Ref. [19]. Model coefficients and aerodynamic coefficients calculated from flight data will be the base extraction of the landing gear influence on aerodynamics in section IV.D. The translational aerodynamic coefficients are given by

$$\begin{aligned} C_{X,\mathrm{meas}} &= (m_{\mathrm{AC}} \cdot a_{x,\mathrm{CG}} - T_{\mathrm{x}})/(\overline{q} \cdot S_{\mathrm{Wing}}), \\ C_{Y,\mathrm{meas}} &= (m_{\mathrm{AC}} \cdot a_{y,\mathrm{CG}} - T_{\mathrm{y}})/(\overline{q} \cdot S_{\mathrm{Wing}}), \\ C_{Z,\mathrm{meas}} &= (m_{\mathrm{AC}} \cdot a_{z,\mathrm{CG}} - T_{\mathrm{z}})/(\overline{q} \cdot S_{\mathrm{Wing}}). \end{aligned} \tag{2}$$

Note that the x, y, and z axes are here the flight mechanics body axes, i.e., with x pointing forward and z pointing downward. These expressions rely on a series of measurements. The accelerometer measurements and especially in the x-axis are crucial to estimate the current forces acting on the aircraft. The total and static pressure measurements are needed to calculate the dynamic pressure $\overline{q}$, but also as part of the thrust model used to determine the engine thrust T

and its components T_x, T_y, and T_z in the body frame. Depending on the engine type, the model usually also require some engine parameters, e.g. the low-pressure fan speed N_1 or the pressure ratio EPR. The quality of the engine model used is obviously of outmost importance for the quality of the aerodynamic force coefficients, especially for $C_{X,\text{meas}}$ and $C_{D,\text{meas}}$.

The lift and drag coefficients ($C_{L,\text{meas}}$ and $C_{D,\text{meas}}$) are then obtained by applying the body to experimental frame coordinate transformation, that is by rotating of these coefficients around the angle of attack and angle of sideslip into the experimental frame as follows:

$$C_{D,\text{meas}} = -\,C_{X,\text{meas}}\,\cos(\alpha) - C_{Z,\text{meas}}\,\sin(\alpha) \tag{3}$$

$$C_{L,\text{meas}} = \;\; C_{X,\text{meas}}\,\sin(\alpha) - C_{Z,\text{meas}}\,\cos(\alpha) \tag{4}$$

Note that the indices *meas* are used to indicate that these aerodynamic coefficient values are extracted from the flight data with the processing steps detailed above. There are, obviously, no sensors that are directly measuring the aerodynamic coefficients.

C. Reference Aerodynamic Model Formulation

The Airbus A320 aerodynamic model is formulated as a two-point model, splitting wing and horizontal tailplane influences, as illustrated in Fig. 9 and explained in detail in [20]. One of the motivation for using such two-point model is that it eases the implementation of local nonlinear effects at the main wing or the tailplane, for instance flow separation effects can be modeled and simulated [21]. Such effects are not relevant for the present work and will therefore be neglected in the following. The rigid body aerodynamic model is based on the well-established derivative model formulation mainly used at DLR for system identification purposes. For example, a version of this formulation was used for the model of the former DLR in-flight simulator ATTAS (VFW 614), which is given in [22] as a result of the system identification process. The Airbus A320 has six different high-lift configurations (FLAP 0, FLAP 1, FLAP 1+F, FLAP 2, FLAP 3, FLAP FULL), which are modeled separately using the aerodynamic model structure given below. The influence on aerodynamics of gear extension is modeled within each high-lift configuration model. The corresponding parameters were estimated separately using only data from flight segments in this configuration.

The lift coefficient C_L is given by the two-point model which consists of the wing/body (WB) and the horizontal tailplane (HT) components:

$$C_L = C_{L,\text{WB}} + C_{L,\text{HT}} \cdot \frac{S_{\text{HT}}}{S_{\text{Wing}}} \cdot \cos(\alpha_{\text{dyn}} - \varepsilon_{\text{HT}}). \tag{5}$$

The wing/body contribution (without ground effect) is given as:

$$C_{L,\text{WB}} = \; C_{L0} + C_{L\alpha,\text{WB}} \cdot \frac{1}{4} \cdot \left(1 + \sqrt{\widehat{X}_0}\right)^2 \cdot \alpha + C_{L,\text{SP}} + C_{L,\text{LG}} \cdot \delta_{\text{LG}} + \Delta C_L(q, \xi, \dots) \tag{6}$$

with $\Delta C_L(q, \xi, \dots)$ being a generic term which encompasses various additional contributions on the aircraft's lift coefficient due to e.g., dynamic effects and controls, which can be and are neglected in the following.

The non-dimensional location of the wing flow separation point $\widehat{X}_0$ without hysteresis effects is defined by (see [23])

$$\widehat{X}_0 = \frac{1}{2}\left(1 - \tanh\left(c_1 \cdot (\alpha - \alpha^\star)\right)\right). \tag{7}$$

The effects of spoilers/airbrakes on the lift coefficient are considered by a combination of the influences of spoilers 2 & 3 and 4 & 5 (numbered from the fuselage to the wing tip). Note, that the innermost spoiler (spoiler 1) is only used on ground and is thus not considered here in the model formulation for the A320 in flight.

$$\begin{aligned} C_{L,\text{SP}} = \;\; & C_{L\alpha,\text{SP}} \cdot \left(\sum_{i=2}^{5} \frac{\delta_{\text{SPRH}\,i} + \delta_{\text{SPLH}\,i}}{2}\right) \cdot \alpha + C_{L\text{SP}23} \cdot \left(\sum_{i=2}^{3} \frac{\delta_{\text{SPRH}\,i} + \delta_{\text{SPLH}\,i}}{2}\right) \\ & + C_{L\text{SP}45} \cdot \left(\sum_{i=4}^{5} \frac{\delta_{\text{SPRH}\,i} + \delta_{\text{SPLH}\,i}}{2}\right). \end{aligned} \tag{8}$$

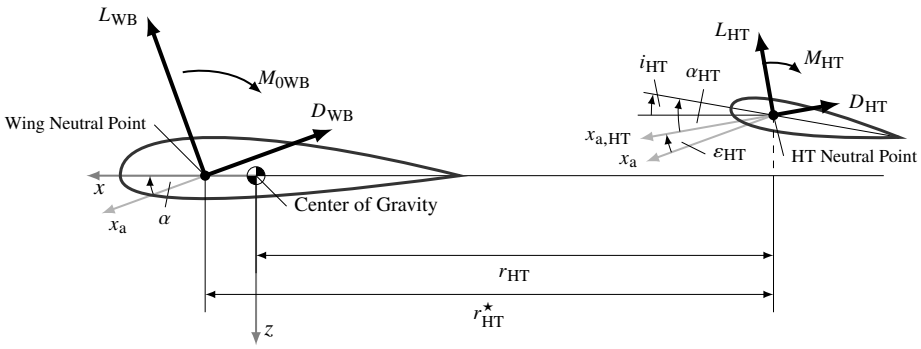

Fig. 9 Wing and horizontal tail geometry for the two-point model formulation, adapted from [20].

The horizontal tailplane lift contribution $C_{L,\mathrm{HT}}$ (without ground effect or jet/slipstream effects) is formulated as:

$$C_{L,\mathrm{HT}} = C_{L0,\mathrm{HT}} + C_{L\alpha,\mathrm{HT}} \cdot \alpha_{\mathrm{HT}} + \Delta C_{L,\mathrm{HT}}(\eta, \dots) \tag{9}$$

where the angle of attack at the tailplane, α_{HT} is given by

$$\alpha_{\mathrm{HT}} = \alpha + \alpha_{\mathrm{dyn}} + i_{\mathrm{HT}} - \varepsilon_{\mathrm{HT}} \tag{10}$$

and the averaged downwash angle $\varepsilon_{\mathrm{HT}}$ at the tailplane's 25% chord line (without consideration of ground effect or wing flow separation) is

$$\varepsilon_{\mathrm{HT}} = \frac{\partial \varepsilon_{\mathrm{HT}}}{\partial \alpha} \cdot \left(\frac{C_{L0}}{C_{L\alpha,\mathrm{WB}}} + \alpha\,(t - \Delta t) \right). \tag{11}$$

The time delay Δt defines the transport delay for the wing downwash to reach the horizontal tailplane and is given by

$$\Delta t = \frac{r^{\star}_{\mathrm{HT}}}{V_{\mathrm{TAS}}}. \tag{12}$$

The dynamic angle of attack (due to pitching) results from

$$\alpha_{\mathrm{dyn}} = \arctan\left(\frac{q \cdot r_{\mathrm{HT}}}{V_{\mathrm{TAS}}} \right). \tag{13}$$

The formula for the drag coefficient C_D is based on a quadratic drag polar formulation in the form of a second-order polynomial expression based on the total lift coefficient C_L and with the zero-lift drag coefficient C_{D0} as constant term. It includes further linear terms modeling further contributions to the total drag e.g., due to airbrakes, ailerons deflections or wing flow separation. Note that the tailplane contribution to the aircraft induced drag is included indirectly through the consideration of the whole aircraft lift coefficient C_L in the drag polar equation. Furthermore, an additional part of the drag equation covers the force related to the rotation of the horizontal tail lift by the local angle of attack α_{HT} acting in direction of the wing/body drag. As only en-route flight points are considered, no ground-effect is considered in the following.

$$\begin{aligned} C_D = \; & C_{D0} + k_1 \cdot C_L + \frac{C_L^2}{e \cdot \pi \cdot \Lambda} + C_{D,\mathrm{SP}} + \frac{\partial C_D}{\partial \widehat{X}} \left(1 - \widehat{X}_0\right) + \underbrace{C_{D,\delta_{\mathrm{LG}}} \cdot \delta_{\mathrm{LG}}}_{C_{D,\mathrm{LG}}} \\ & - C_{L,\mathrm{HT}} \cdot \frac{S_{\mathrm{HT}}}{S_{\mathrm{Wing}}} \cdot \sin(\alpha_{\mathrm{dyn}} - \varepsilon_{\mathrm{HT}}) + \Delta C_D(\beta, \xi, \dots) \end{aligned} \tag{14}$$

Within this standard formulation of the drag coefficient, the gear influence $C_{D,\mathrm{LG}}$ is considered as a linear model parameter $C_{D,\delta_{\mathrm{LG}}}$ switched on and off by the binary gear flag δ_{LG} resulting from the gear signals (e.g., "down and locked" or "gear down command") in the flight data or from simulation. The gear influence can also be made artificially

continuous by replacing the binary signal δ_{LG} by a continuous one: for instance going linearly from zero to one (or the other way around) with a well-chosen rate during extension (or retraction). As it will be seen later, the more complex evolution of the drag induced by the landing gear during extension or retraction that is at core of the present work can be represented by a more complex evolution of δ_{LG}, for instance as a nonlinear function of the positions of the gear doors and of the landing gear legs.

The effects of spoilers/airbrakes on the drag coefficient are considered by a combination of the influences of spoilers 2 & 3 and 4 & 5.

$$C_{D,\mathrm{SP}} = \; C_{D,\mathrm{SP},23} \cdot \left(\sum_{i=2}^{3} \frac{\delta_{\mathrm{SP\,RH}\,i} + \delta_{\mathrm{SP\,LH}\,i}}{2} \right) + C_{D,\mathrm{SP},45} \cdot \left(\sum_{i=4}^{5} \frac{\delta_{\mathrm{SP\,RH}\,i} + \delta_{\mathrm{SP\,LH}\,i}}{2} \right) \tag{15}$$

Note that different model coefficients (e.g., C_{L0}, $C_{L\alpha,\mathrm{WB}}$, $C_{L,\mathrm{SP}}$, $C_{L\alpha,\mathrm{HT}}$, or C_{D0}) are corrected for Mach number effects using a Prandtl-Glauert correction. The parameters for this model are estimated using the flight data evaluation process for flight performance model determination described in detail in Refs. [6, 15, 16, 24].

D. Extraction of Landing Gear Influence on Drag from Flight Data

To extract the gear influence on aircraft drag during extraction from the aerodynamic data calculated in Eqs. (2–4), all other parts contributing to the drag must be eliminated. In a first step, the aerodynamic drag model presented in the previous section is further simplified by neglecting the flow separation effects and influences from e.g., pitching rate, sideslip or aileron deflection:

$$\begin{aligned} C_{D,\mathrm{model}} = \; & C_{D0} + k_1 \cdot C_L + \frac{C_L^2}{e \cdot \pi \cdot \Lambda} + C_{D,\mathrm{SP}} + \cancelto{0}{\frac{\partial C_D}{\partial \widehat{X}} \left(1 - \widehat{X}_0\right)} + C_{D,\mathrm{LG}} \\ & - C_{L,\mathrm{HT}} \cdot \frac{S_{\mathrm{HT}}}{S_{\mathrm{Wing}}} \cdot \sin(\alpha_{\mathrm{dyn}} - \varepsilon_{\mathrm{HT}}) + \cancelto{0}{\Delta C_D(\beta, \xi, \dots)} \end{aligned} \tag{16}$$

$$C_{D,\mathrm{model}} \approx \widetilde{C}_D = \underbrace{C_{D0} + k_1 \cdot C_L + \frac{C_L^2}{e \cdot \pi \cdot \Lambda} + C_{D,\mathrm{SP}} - C_{L,\mathrm{HT}} \cdot \frac{S_{\mathrm{HT}}}{S_{\mathrm{Wing}}} \cdot \sin(\alpha_{\mathrm{dyn}} - \varepsilon_{\mathrm{HT}})}_{C_{D,\text{model w/o gear}}} + C_{D,\mathrm{LG}} \tag{17}$$

In the light of the model derived above, Eq. (1) is expanded to include effects that are approximated, neglected, or that cannot be not controlled.

$$C_{D,\mathrm{LG}} = \left(C_{D,\mathrm{meas}} - C_{D,\text{meas error}}\right) - \left(C_{D,\text{model w/o gear}} + C_{D,\text{model neglected terms}} - C_{D,\text{model error}}\right) \tag{18}$$

Apart from the sum of the neglected terms $C_{D,\text{model neglected terms}}$, which are explicitly neglected because of their very small values in practice for the considered time segments, it is harder to control the other terms: $C_{D,\text{meas error}}$ and $C_{D,\text{model error}}$. The former, $C_{D,\text{meas error}}$, is induced by all potential sources of error affecting the determination of $C_{D,\mathrm{meas}}$ as expressed in Eq. (3). This includes the errors due to the thrust model and due to air-data and accelerometer sensor measurement errors. The mitigation strategy is to use a well-calibrated thrust model and to try to detect abnormal measurements and exclude the corresponding time segments. As the data used comes from operational flights, a specific calibration of the air data sensors for each individual aircraft is not practicable, so the regular calibration of these sensor will have to be sufficient. The latter term, $C_{D,\text{model error}}$, consists in the model error which would be present even without model simplifications. The amount of error made is difficult to estimate, but the mitigation strategy consists in identifying good performance models for the aircraft, before considering the identification of the drag caused by the landing gear. For this, extensive work has been performed, as shown in [6].

Eventually, by combining Eq. (1) and (17), the following estimate $\widehat{C}_{D,\mathrm{LG}}$ is obtained:

$$\widehat{C}_{D,\mathrm{LG}} = C_{D,\mathrm{meas}} - \left(C_{D0} + k_1 \cdot C_L + \frac{C_L^2}{e \cdot \pi \cdot \Lambda} + C_{D,\mathrm{SP}} - C_{L,\mathrm{HT}} \cdot \frac{S_{\mathrm{HT}}}{S_{\mathrm{Wing}}} \cdot \sin(\alpha_{\mathrm{dyn}} - \varepsilon_{\mathrm{HT}}) \right) \tag{19}$$

Note that the aerodynamic coefficients are not corrected for Mach number effects in this case because in the considered flight data the landing gear is only extended during low-speed flight conditions for which the assumption of

incompressible flow is valid. For the evaluation, the drag coefficient estimate $\widehat{C}_{D,\mathrm{LG}}$ is calculated for the whole gear extension sequence of each flight and the corresponding time series is then further processed to derive a model from it.

Following the processing steps defined above, the data from the 804 gear extension maneuvers were analyzed. Figure 10 shows the time series of 804 landing gear drag estimates data segments with gray lines. The number of lines and the fact that each is fairly noisy yields an almost contiguous gray area, with irregular borders. Even though it is noisy, it appears clearly that there is an underlying signal to be found: the gray area shows, besides evident noisy individual time series, clear and consistent variations across all 804 time series. The average estimate from those 804 time series is represented in with the thick black line, along with the 2-σ bands. Their trend and spacing are consistent with the visual impression provided by the overall evolution of the individual gray lines.

The gear drag coefficient estimates, both individually and on average, clearly reflect a sequence of actions with a nonlinear and complex change of drag during the about 17 s of the gear extension (see section II). A first noticeable drag increase starts around 1 s after the "gear down" command. This ramp-like increase ends after less than 1 s, leading to a plateau at a slightly elevated drag level which presumably corresponds to the opening of the gear doors and the drag increase due to the exposure of the doors to the flow under the airframe and due to the opened gear bays at all three gears. After that, a more significant increase of the gear drag coefficient estimate starts at about 4 s and lasts for another 4 s. It is followed by a almost flat segment for around 7 s (until about 15.5 to 16 s). This plateau is assumed to correspond to the relatively long duration of the gear leg rotation, between the moment at which the gears are fully exposed to the external flow until they lock in extended position. At the end of the sequence, at about 16 s, the gear drag coefficient estimate decreases again, presumably as a result from the closing of the gear doors.

At about 4 s, at the kink between the first plateau corresponding to the opening of the gear doors, and the main drag increase, a couple of periods of a sawtooth profile can be seen. This sawtooth profile is not very pronounced and could simply be left out of the model without loosing much precision. The authors' educated guess is that this corresponds to specific events during the initial motion of the main gears. The main gear kinematics is such that at specific angles of the gear leg, each of the two wheels are in one of the following situations (cf. Fig. 5): (1) inside the gear bay, (2) at the entrance of the gear bay and partly blocking the flow, thereby reducing the drag increase due to the open storage bay, (3) right outside of the gear bay causing drag and possibly even redirecting part of the flow towards the landing gear storage bay, (4) fully exposed to the outside flow. Following this interpretation, the sawtooth profile would correspond to the successive drag positive and negative increments as the two wheels of the main gear passing successively through these four positions.

The average drag estimate value $\overline{C}_{D,\mathrm{LG}}$ does not start at zero at $t = 0\,s$, but shows a small negative offset $\Delta C_D(t = 0\,s) = -0.00275$. This most likely results from aerodynamic or thrust model errors. Nevertheless, the successive increments during the gear extension can be analyzed independently of the overall level. Considering the difficulty of analyzing drag on such short and relatively unsteady flight maneuvers, this offset remains very reasonable.

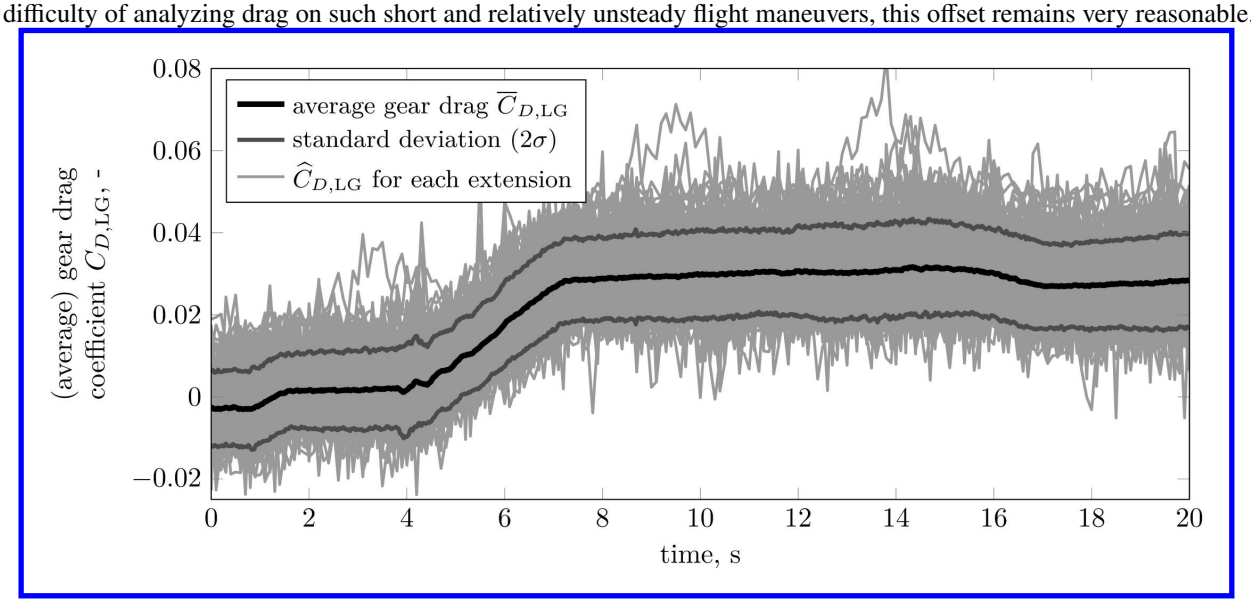

Fig. 10 Gear drag coefficient from flight data based 804 extracted data sets: gear drag coefficient calculated flight data and the available aerodynamic model (gray lines), average drag coefficient (thick black line) and corresponding standard deviation (dark gray lines).

V. Modeling of the Gear-Induced Drag

A. Definition of the Kinematics Parameters

Multiple parts are moving throughout the gear extension or retraction. The ones that are relevant for the drag model are the nose gear doors, main gear doors, nose gear leg, and main gear legs. As the nose gear doors are significantly smaller than the main gear doors and, similarly, the nose gear bay is also significantly smaller than the main gear bays, it was decided to not model their individual contributions to the drag separately, but rather to define only one parameter for them. The definition of the kinematics parameters for the main gear leg (δ_{MG}), the nose gear leg (δ_{NG}), and the doors (δ_{doors}) are defined below. For each of the three parameters, the ranges of values that they can take were defined based on common sense and based on pictures and cutaway diagrams.

The main landing gear angle δ_{MG} is defined as equal to 90° when the leg is fully extended (approximately parallel to the aircraft symmetry plane) and equal to 15° when the leg is fully retracted. In the fully retracted position, the main landing leg remains at an angle compared to the body (x_b, y_b) plane which was estimated to be 15°. Even if the rotation of the main gear leg is not exactly contained in the aircraft body (y_b, z_b) plane, the defined main landing gear angle δ_{MG} corresponds roughly to the angle between the leg and the body (x_b, y_b) plane. Both left and right gears use this definition, ignoring the fact they rotate in opposite directions.

The nose gear angle δ_{NG} is not defined with respect to the horizontal plane and vertical direction, but based on its position when retracted. When retracted, the nose gear wheel axle is above the leg rotation point (the gear leg is pointing forward and slightly upward). When extended, the nose gear leg is not fully vertical either, but rather slightly pointing forward. In the end, the total rotation angle between these two positions appears to be approximately 90°, so it seemed very natural to choose the following definition for the nose gear angle: $\delta_{\text{NG}} = 0°$ for the retracted position and $\delta_{\text{NG}} = 90°$ for the extended position.

The gear door angle δ_{doors} is defined based on the kinematics of the main gear doors. As it can be seen in Fig. 5, these doors cover mostly the flat bottom of the center box belly and also slightly extend to the side of the center box with a rounded transition in between. The portion of the doors that constitutes the bottom of the aircraft belly is roughly horizontal when the door is closed and roughly vertical when the door is fully opened. So, naturally, the gear door angle δ_{doors} was defined as $\delta_{\text{doors}} = 0°$ for the closed position and $\delta_{\text{doors}} = 90°$ for the fully opened position.

Table 3 Minimum and maximum values for the kinematic parameters.

position	gear doors (δ_{doors})	nose gear (δ_{NG})	main gear (δ_{MG})
closed/retracted (min)	0°	0°	15°
opened/extended (max)	90°	90°	90°

B. Overall Structure of the Model

The landing gear extraction sequence is composed of different steps relevant for its influence on the aircraft drag, and the kinematic parameters δ_{doors}, δ_{NG}, and δ_{MG} defined in the previous section will be used to define the nonlinear evolution of the various contributions to the drag. The overall landing gear drag coefficient is defined as the superposition of three individual contributions:

$$\begin{aligned}\widetilde{C}_{D,\text{LG}} : [\delta_{\text{doors,min}}, \delta_{\text{doors,max}}] \times [\delta_{\text{NG,min}}, \delta_{\text{NG,max}}] \times [\delta_{\text{MG,min}}, \delta_{\text{MG,max}}] &\to \mathbb{R} \\ \widetilde{C}_{D,\text{LG}}(\delta_{\text{doors}}, \delta_{\text{NG}}, \delta_{\text{MG}}) &\mapsto C_{D,\text{doors}}(\delta_{\text{doors}}) + C_{D,\text{NG}}(\delta_{\text{NG}}) \\ &\quad + C_{D,\text{MG}}(\delta_{\text{MG}}) \, .\end{aligned} \tag{20}$$

Note that for conciseness, no distinction between left and right main landing gear doors and legs is made. Splitting these terms into two equally large terms and using different kinematics parameters for each main gear door and leg would be trivial and would allow simulating a reduced drag in case of partial failure. For instance a door could open, but the gear leg fails to unlock. The door could also fail to unlock on one side.

C. Parametrized Model for the Landing Gear Door Drag

The door influence on the drag $C_{D,\text{doors}}$ is formulated as the following nonlinear function of the δ_{doors} angle:

$$\begin{aligned} C_{D,\text{doors}}: \quad [\delta_{\text{doors,min}}, \delta_{\text{doors,max}}] &\rightarrow [0, C_{D,\text{doors,nom}}] \\ C_{D,\text{doors}}(\delta_{\text{doors}}) &\mapsto \min\left(1, \frac{\delta_{\text{doors}} - \delta_{\text{doors,min}}}{\delta_{\text{doors,nom}} - \delta_{\text{doors,min}}}\right) C_{D,\text{doors,nom}} \,, \end{aligned} \tag{21}$$

with $C_{D,\text{doors,nom}}$ being the drag coefficient increment when the doors are fully open and $\delta_{\text{doors,nom}}$ being an *effective* door angle at which the drag increment $C_{D,\text{doors,nom}}$ induced by the door and the aerodynamics of the opened gear bay is first reached. Logically the condition $\delta_{\text{doors,nom}} \leq \delta_{\text{doors,max}}$ holds.

The rationale for choosing this model structure is the following. At the beginning of the opening motion, a progressive increase of the drag is expected and a linear dependency with the door angle δ_{doors} is used. The final/total drag increment $C_{D,\text{doors,nom}}$ is however expected to be reached already at an angle $\delta_{\text{doors,nom}}$ rather closer to $\delta_{\text{doors,min}}$ than to $\delta_{\text{doors,max}}$. Note that the purpose of this section is to select a potential candidate for the model structure, but the determination of adequate parameter values, in this case for $\delta_{\text{doors,nom}}$ and $C_{D,\text{doors,nom}}$, will be determined in a second step. The mathematical expression in Eq. (21) defines a piecewise linear function with two intervals:

- For $\delta_{\text{doors}} \in [\delta_{\text{doors,min}}, \delta_{\text{doors,nom}})$, $C_{D,\text{doors}}(\delta_{\text{doors}})$ increases linearly with δ_{doors} from 0 to $C_{D,\text{doors,nom}}$.
- For $\delta_{\text{doors}} \in [\delta_{\text{doors,nom}}, \delta_{\text{doors,max}}]$, $C_{D,\text{doors}}(\delta_{\text{doors}})$ remains constant: $C_{D,\text{doors}}(\delta_{\text{doors}}) = C_{D,\text{doors,nom}}$.

D. Parametrized Model for the Nose Landing Gear Drag

For the modeling of the drag induced by the nose gear $C_{D,\text{NG}}$ a similar idea as for the gear doors is used. However, two separate contributions are considered: one for the wheels ($C_{D,\text{NG,wheels}}$) and one for the leg ($C_{D,\text{NG,leg}}$):

$$\begin{aligned} C_{D,\text{NG}}: \quad [\delta_{\text{NG,min}}, \delta_{\text{NG,max}}] &\rightarrow \mathbb{R} \\ C_{D,\text{NG}}(\delta_{\text{doors}}, \delta_{\text{NG}}, \delta_{\text{MG}}) &\mapsto C_{D,\text{NG,wheels}}(\delta_{\text{NG}}) + C_{D,\text{NG,leg}}(\delta_{\text{NG}}) \,. \end{aligned} \tag{22}$$

The reason for this distinction is that the wheels are already outside of the gear bay very early during the rotation of the gear leg, so their contribution to the gear drag is expected to grow rapidly and then to remain constant for the remainder of the rotation. A similar model structure as for the landing gear doors is selected, with a nonlinear function of the nose gear leg angle δ_{NG}:

$$\begin{aligned} C_{D,\text{NG,wheels}}: \quad [\delta_{\text{NG,min}}, \delta_{\text{NG,max}}] &\rightarrow [0, C_{D,\text{NG,wheels,nom}}] \\ C_{D,\text{NG,wheels}}(\delta_{\text{NG}}) &\mapsto \min\left(1, \frac{\delta_{\text{NG}} - \delta_{\text{NG,min}}}{\delta_{\text{NG,wheels,nom}} - \delta_{\text{NG,min}}}\right) C_{D,\text{NG,wheels,nom}} \,. \end{aligned} \tag{23}$$

At the beginning of the extension, the gear leg is almost aligned with the flow. During the rotation of the leg, it progressively becomes almost perpendicular to the flow and its impact on the drag is therefore expected to be continuously growing throughout the rotation. Based on this geometrical consideration, it would be logical to use a sine function to describe the leg cross-section and to use this cross-section for modeling the drag. At the same time, the leg certainly has complex aerodynamic interactions with the opened nose gear bay and the wheels, so it remains unclear whether using the cross-section would provide the right dependency. In a first step, a simple linear dependency with the nose gear kinematic parameter δ_{NG} is used. Even if the results shown later do not allow analyzing the separate contributions of each gear and of the doors separately, the results are very close to the experimental data and using a more complicated formula does not seem useful.

$$\begin{aligned} C_{D,\text{NG,leg}}: \quad [\delta_{\text{NG,min}}, \delta_{\text{NG,max}}] &\rightarrow [0, C_{D,\text{NG,wheels,nom}}] \\ C_{D,\text{NG,leg}}(\delta_{\text{NG}}) &\mapsto \frac{\delta_{\text{NG}} - \delta_{\text{NG,min}}}{\delta_{\text{NG,max}} - \delta_{\text{NG,min}}} C_{D,\text{NG,leg,nom}} \,. \end{aligned} \tag{24}$$

E. Parametrized Model for the Main Landing Gear Drag

The main gear extension is assumed to have a more complex influence on the drag than the doors or the nose gear, due to its kinematics, geometry, and the large parts that progressively exit their storage bays in the wing and the belly of the aircraft. As shown in Fig. 5, the main gear extension includes the opening of a slot in the lower surface of the wing, where the main gear leg is stored when retracted. During the rotation of the leg, the two wheels successively exit the wheel bays and become exposed to the airflow. Once both wheels are out of their bays in the belly of the aircraft, they are assumed to already generate roughly the same drag as for the remaining part of the main gear leg rotation.

The aerodynamic interaction between the wheels and the corresponding opened main landing gear bay is expected to cause complex variations of the drag, even if the amplitude of these variations is not easy to predict. At some angles, one of the wheels can be almost covering/blocking the hole of the opened bay, which tends to alleviate the drag that this opened bay induces. At other angles, the wheel may on the contrary deflect part of the airflow toward the opened main landing gear bay in a way that might reinforce its impact on drag. To allow a fairly complex evolution of the drag during the rotation of the gear leg, the main gear drag coefficient $C_{D,\mathrm{MG}}$ is modeled by defining a nonlinear effectiveness function $f_{\mathrm{MG}} : [\delta_{\mathrm{MG,min}}, \delta_{\mathrm{MG,max}}] \rightarrow [-0.1, 1.0]$ of the gear leg angle and using it as a scaling factor in front of the corresponding parameter $C_{D,\mathrm{MG,nom}}$. Allowing f_{MG} to be negative makes it possible to model up to a 10% $C_{D,\mathrm{MG,nom}}$ drag reduction when the wheels are almost blocking the entrance of the left and right main landing gear bays. With this, the nonlinear function $C_{D,\mathrm{MG}}$ reads:

$$\begin{aligned} C_{D,\mathrm{MG}}(\delta_{\mathrm{MG}}) : \quad [\delta_{\mathrm{MG,min}}, \delta_{\mathrm{MG,max}}] \quad &\rightarrow \quad [-0.1\, C_{D,\mathrm{MG,nom}}, C_{D,\mathrm{MG,nom}}] \\ C_{D,\mathrm{MG}}(\delta_{\mathrm{MG}}) \quad &\mapsto \quad f_{\mathrm{MG}}(\delta_{\mathrm{MG}})\, C_{D,\mathrm{MG,nom}} \,. \end{aligned} \tag{25}$$

In this work, the nonlinear effectiveness function f_{MG} is defined and implemented as a one-dimensional lookup-table whose support vectors and values will be estimated (see section V.F.5).

F. Estimation of the Parameter Values

A number of parameters are foreseen in the model structure and the individual terms defined in the previous sections. These parameters are used to get the model to closely match the evolution of the drag coefficient extracted from the flight data and shown in Fig. 10. During this work, no specific method or software was used to retrieve the model parameters, for instance optimization or parameter estimation. The parameters defined above could be either directly estimated from the drag evolution plot or were quick to estimate with a couple of trials. A state-of-the-art parameter estimation technique could be used to further enhance the model quality, even if it does not seem to be worth the effort for this application.

Table 4 Definition of doors and gears extension model parameters ($t = 0\,s$ defined as gear down command).

	gear doors		nose gear	main gear
	opening	closing	extension	extension
start	0.8 s	15.5 s	3.1 s	3.1 s
end	2.5 s	17.2 s	15.6 s	15.6 s
duration	1.7 s	1.7 s	12.5 s	12.5 s
rate	52.94°/s	−52.94°/s	7.20°/s	6.00°/s

1. Estimated Values for the Kinematic Parameters

The first step consists in defining the time-evolution of the kinematic parameters δ_{doors}, δ_{NG}, and δ_{MG} defined in section V.A. Based on the video recording each of these kinematic parameters seem to varying during specific time intervals and at constant speed (the brief initial pause for the leg motion is neglected). The start and end times for each motion are summarized in Table 4 with the corresponding time-derivatives $\dot{\delta}_{\mathrm{doors}}$, $\dot{\delta}_{\mathrm{NG}}$, and $\dot{\delta}_{\mathrm{MG}}$ of the kinematics parameters. The time history of these parameters can be seen in the bottom three plots in Fig. 11. The numerical values from Table 4 were initially estimated based on the video recording and later slightly adjusted to improve the match with the flight data.

2. Estimated Values for the Nominal Gear/Door Drag Parameters

Before modeling the nonlinearities in the drag coefficient evolution, the next step consists in analyzing the different relatively constant levels in the time-evolution from Fig. 11. From the aerodynamic model identification performed in [6], the total gear-induced drag coefficient values for three different high lift system configurations (FLAP 2, 3, and FULL) are known. These values are provided in Table 5a.

The gear drag coefficient values for the three configurations are within $0.299 \pm 4\%$, therefore no dependency on the high-lift configuration is considered and the average value $\overline{C}_{D,\delta_{\mathrm{LG}}} = 0.0299$ is selected for all configurations. Looking to Fig. 10 it is directly visible that the average value $\overline{C}_{D,\delta_{\mathrm{LG}}}$ of approx. 0.03 resulting from the available aerodynamic model is well matching the difference between the average gear drag coefficient at 0 s (beginning of the sequence) and 17 s (end of sequence) with gear down and locked. No information was found which allows estimating the correct split between the drag due to the main gear, to the nose gear wheels, and to the nose gear leg. A split with respectively 75%, 20%, and 5% of the total gear drag coefficient $\overline{C}_{D,\delta_{\mathrm{LG}}}$ is assumed, leading to the values provided in Table 5b. This split could easily be revised, if further information becomes available.

The value for the door drag coefficient $C_{D,\mathrm{doors}} = 0.0043$ (Table 5c) could be directly extracted from Fig. 10. It corresponds to the difference between the drag during the plateau for $t \in [1.8\,s, 3.8\,s]$ and the drag at the beginning of the sequence as well as to the difference between the quasi-plateau for $t \in [8\,s, 15.5\,s]$ and the quasi-plateau at the end of the sequence.

Table 5 Nominal drag coefficient values

(a) Gear drag coefficient values from [6]

high lift config.	$C_{D,\delta_{\mathrm{LG}}}$
FLAP 2	0.0296
FLAP 3	0.0291
FLAP FULL	0.0311

(b) Assumed gear drag coefficient split

gear	value	factor
$\overline{C}_{D,\delta_{\mathrm{LG}}}$	0.0299	1.00
$C_{D,\mathrm{MG}}$	0.0224	0.75
$C_{D,\mathrm{NG,wheels}}$	0.0060	0.20
$C_{D,\mathrm{NG,leg}}$	0.0015	0.05

(c) Drag coefficient for the doors

doors	value
$C_{D,\mathrm{doors}}$	0.0043

3. Estimated Value for $\delta_{doors,nom}$

Based on the average drag evolution shown in Fig. 10, the duration of the initial ramp during the opening of the doors was estimated to be approximately 0.65 s. Based on the angular rate of the main landing gear doors, the value $\delta_{\mathrm{doors,nom}}$ at which the doors-induced nominal drag increase $C_{D,\mathrm{doors,nom}}$ is reached was set to 35°.

By comparing in Fig. 10 the rate at which the initial increase of the drag occurs and the comparatively low rate of drag decrease when the doors are closing, it was decided to use a different value during the closing motion: $\delta_{\mathrm{doors,nom}} = 90°$. Based on the data available, there is no significant difference in the door rotational rate between the opening and closing motions. Whilst the authors have no physical explanation for the difference in drag increase/decrease rates, setting different values for opening and closing motions provides a good match with the flight data.

4. Estimated Value $\delta_{\mathrm{NG,wheels,nom}}$

Based on similar analysis, the value $\delta_{\mathrm{NG,wheels,nom}}$ at which the drag induced by the nose wheel was also set at 35°. No gear retraction sequence was considered in this analysis, such that it was not possible to analyze whether the drag decrease rate upon retraction matches the drag increase rate upon extension. Besides, the data do not allow distinguishing between main gear and nose gear effects, so this value, just as the split proposed in Table 5b, should rather be interpreted as an educated guess made by the authors than supported by concrete evidence.

5. Estimated Values for the $f_{\mathrm{MG}}(\delta_{\mathrm{MG}})$ Lookup-Table

As explained in section V.E, the nonlinear drag evolution $C_{D,\mathrm{MG}}(\delta_{\mathrm{MG}})$ is modeled as the product of a constant main gear drag coefficient for the fully extended position and a one-dimensional lookup-table $f_{\mathrm{MG}}(\delta_{\mathrm{MG}})$. Based on the results in Fig. 10, a discretization of the input range ($\delta_{\mathrm{MG}} \in [15°, 90°]$) was made. For this, points were introduced where slope changes in the main landing gear drag occur. A value was also set for each of these points. Eventually, the lookup-table shown in Table 6 was obtained.

Table 6 Lookup-table of the $f_{\mathrm{MG}}(\delta_{\mathrm{MG}})$ factor and of the corresponding drag coefficient value $C_{D,\mathrm{MG}}(\delta_{\mathrm{MG}})$.

extension angle δ_{MG}	$f_{\mathrm{MG}}(\delta_{\mathrm{MG}})$		drag coefficient $C_{D,\mathrm{MG}}(\delta_{\mathrm{MG}})$
15.0°	0.00		0.0000
16.0°	0.01		0.0002
18.9°	−0.01		−0.0002
19.8°	−0.06	⇒	−0.0013
21.4°	0.05		0.0011
22.8°	0.00		0.0000
39.6°	0.93		0.0208
70.0°	0.95		0.0213
90.0°	1.00		0.0224

VI. Results

To verify that the model of the drag during the gear extension sequence matches the flight data, the sequence is simulated and the model is evaluated throughout the simulation. Based on the kinematic parameters defined in section V.A and the associated numerical values from section V.F.1, the time series of the kinematic parameters are fully defined. All other parts of the drag model defined in section V are algebraic functions or terms: there is no dynamic element or state. In the end, the model of the gear/doors-induced drag coefficient increment is the algebraic and highly nonlinear function $\widetilde{C}_{D,\mathrm{LG}}(\delta_{\mathrm{doors}}, \delta_{\mathrm{NG}}, \delta_{\mathrm{MG}})$ defined in Eq. (20).

This means that, once the time series for the three kinematics parameters δ_{doors}, δ_{NG}, and δ_{MG} is known, the evaluation of the model can be made individually for each time (no numerical integration needed):

$$\forall t \in [0, t_{\mathrm{end}}],\ C_{D,\mathrm{LG,model}}(t) = \widetilde{C}_{D,\mathrm{LG}}\left(\delta_{\mathrm{doors}}(t), \delta_{\mathrm{NG}}(t), \delta_{\mathrm{MG}}(t)\right) \tag{26}$$

The result is shown in Fig. 11. In this figure, the first subplot shows the match between the average gear drag coefficient extracted from the operational flight data and the prediction of the proposed model. The time series of the kinematic parameters are shown in the other three subplots. The match is very good, showing that the limited number of parameters chosen and manually tuned are largely sufficient to reproduce the nonlinear drag evolution during the gear extension. Note that the nonlinear evolution of the drag is not very complicated and would be very easy to generate a model that perfectly matches the flight data. Note that also that in this plot, the average drag is corrected for the aforementioned offset ΔC_D for better comparability.

To better evaluate the differences between the flight data and the gear drag predicted by the model, the difference between these two values is shown in Fig. 12. The overall error is very small with peaks less than 10% in general. During the drag increase between 4 s and 8 s in the sequence the model has still some deficiencies, which could be addressed for example in further identification of the main gear effectiveness function f_{MG}. This deviation between model and flight data should however not be overemphasized: during this time interval, the rapid increase in gear drag coefficient occurs at a rate of about 0.009 -/s, so just by shifting one of these curves by roughly 100 ms a similarly large absolute deviation would be obtained during that phase.

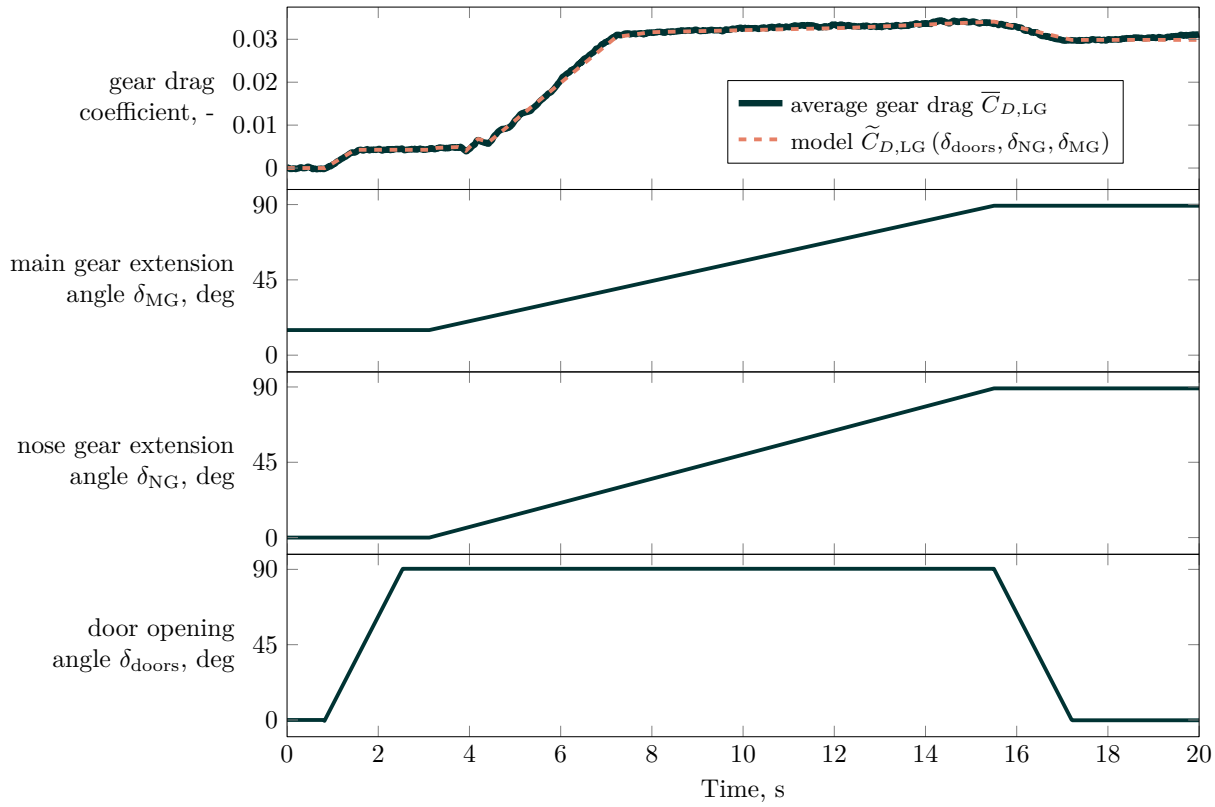

Fig. 11 Time history of model results: average gear drag coefficient $\overline{C}_{D,\mathrm{LG}}$ from flight data and model $\widetilde{C}_{D,\mathrm{LG}}$ (top); simulated main gear and nose gear extension angle (two plots in the middle); simulated gear door opening angle (bottom).

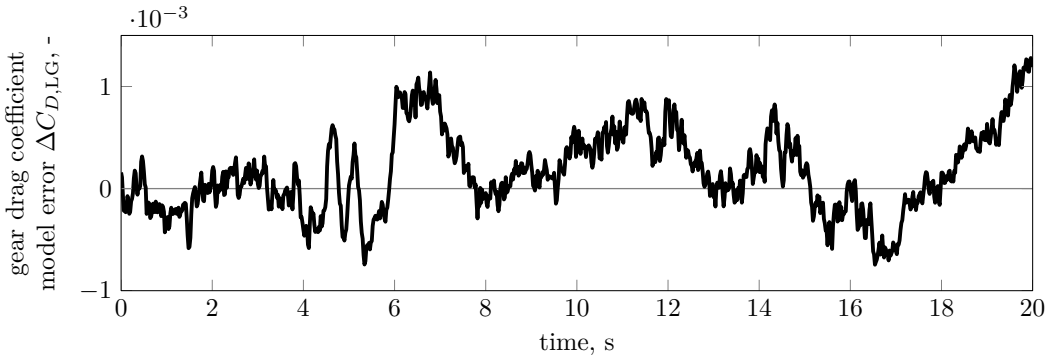

Fig. 12 Gear drag coefficient model error $\Delta C_{D,\mathrm{LG}}$ during the extension sequence.

In practice, even larger errors could be tolerated as it is not clear that there is a practical need for the level of precision reached (hence, also the limited need for even better match with numerical optimization of the parameters), especially considering that even with:

- the effort spent in tuning the performance models (aerodynamics with and without gear, propulsion) used to indirectly obtain the drag coefficient out of the operational flight data,
- the consideration of recordings of 804 gear extensions, and
- the effort spent in attempting to correct potential synchronization issue

the average gear drag coefficient evolution remains most certainly not nearly as accurate as the match between between the numerical model and this drag coefficient evolution is already.

After the gear is fully extended and locked and the doors are closed again (after 18 s), there is an increase in drag visible which is not covered by the model and hence is reflected as model error in Fig. 12. However, the last two seconds of the time series correspond to the flight after the gear is extended, which often contains further maneuvers (e.g., glideslope intercept) and are not relevant for the evaluation of the gear model.

Finally, Fig. 13 shows a comparison of the complex nonlinear drag change during the gear extension sequence and a fairly typical implementation with a simple linear increase is being made between 0 and the final gear drag value over the entire duration of the gear extension. At the beginning of the sequence, both model approaches give comparable results until approx. 5 s, but afterwards, the linear derivative model largely underpredicts the drag change (retrieved from flight data). There are undoubtedly plenty of other implementations of this transition in simulators: jump or ramp between the two values at any point during the extension (e.g., very early based on the gear lever signal, after the gear unlock flag is received, when the gear down locked signal is received, etc.). It seems rather unlikely that many simulator model designers implemented a gear drag evolution profile somewhat close to the time series that was found in the flight data.

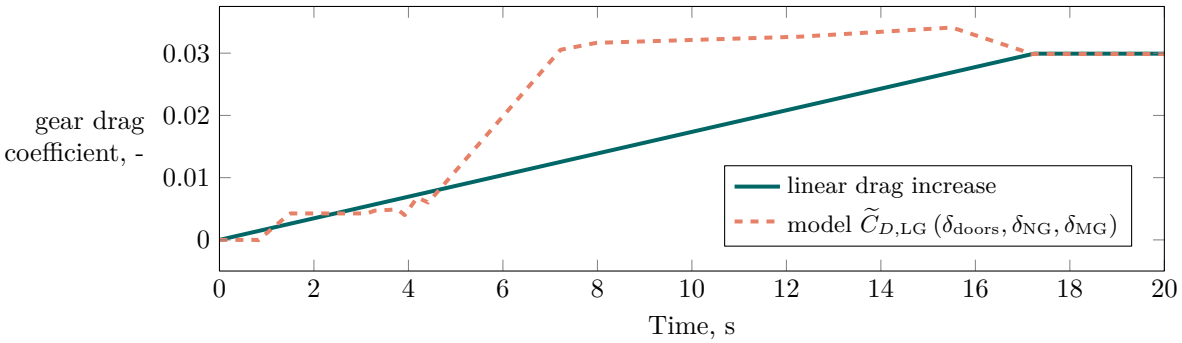

Fig. 13 Comparison between the proposed nonlinear model of the gear drag during the extension sequence and a presumably more common linear interpolation between start and final values over the same time interval.

VII. Summary and Outlook

This paper describes a model of the drag change during the landing gear extension of an Airbus A320neo. To obtain the gear contribution to the overall drag from flight data, the most logical and common approach is to compare the drag coefficient values obtained for the two possible configurations: with extended gear or with retracted gear. This is fairly common in the area of aircraft system identification. However, models able to predict the drag during the transition between these two configurations could not be found in the literature. Whilst the authors do not claim to be the first to propose such a model, they could not find any published model of the drag during the gear extension (or retraction). The proposed model is provided with all necessary numerical values. It is applicable to the Airbus A320 family, which is presently the most sold airliner of all times.

The method used to generate this model is detailed and certainly applicable to other aircraft types. Based on an available operational flight data set, the relevant data about the landing gear deployment was extracted and further used for the model determination. Using the aerodynamic coefficients calculated from flight data together with information about the engine thrust and a predetermined aerodynamic model of the Airbus A320neo, the aircraft drag variation during the landing gear extension sequence was calculated during 804 airport approaches. The high number of gear extension sequences is crucial to obtain good reference data, as each of them is affected by significant disturbances (noise, atmospheric turbulence) and effects linked to dynamic maneuvers from the pilot or autopilot.

The proposed model shows a very good match with the resulting average drag coefficient variation during the landing gear extension retrieved from flight data, including previously not considered effects of, e.g., gear door opening and closing. The results show that the gear drag evolution during extension is rather unsteady, with three main ramps (two positive and one negative) with fairly long phases with constant drag in between. A linear interpolation between the drag levels with retracted gear and the drag level with extended gear would, depending on its exact implementation, rather underestimate the gear-induced drag during most of the duration of the gear extension.

Future work might include a further estimation of model parameters for the drag during gear extension, application of the same strategy to, e.g., the deployment of high-lift system devices to better predict any non-linear behavior in simulation. Furthermore, the presented model for the landing gear drag change could be linked to a kinematic model of

the landing gear to further enhance the physical link between the landing gear geometry and the drag variation (e.g., analyzing the cross-section and exact location of the different parts throughout the extension). The flight data used did not allow the identification of the pitching and yawing moment linked to each gear and door. This said, the analysis of the kinematics would allow the derivation of plausible pitching and yawing moments from the drag model proposed in this work.

Acknowledgments

The authors warmly thank DLR's test pilot Jens Heider and the research flight department in Braunschweig for providing the maintenance video of DLR's Airbus A320 ATRA used to reveal the gear extension sequence used in this work.

References

[1] *Certification Specifications for Aeroplane Flight Simulation Training Devices 'CS-FSTD(A)"*, EASA, May 2018. URL https://www.easa.europa.eu/en/document-library/certification-specifications/cs-fstda-issue-2.

[2] Morelli, E. A., "Flight Test Maneuvers for Efficient Aerodynamic Modeling," American Institute of Aeronautics and Astronautics, Inc. (AIAA), Portland, Oregon, USA, 2011.

[3] Grauer, J. A., "Real-Time Parameter Estimation Using Output Error," AIAA Atmospheric Flight Mechanics Conference, American Institute of Aeronautics and Astronautics, Inc. (AIAA)American Institute of Aeronautics and Astronautics, Inc. (AIAA), Atlanta, Georgia, USA, 2014. doi:10.2514/6.2014-2556.

[4] Lichota, P., Sibilski, K., and Ohme, P., "D-Optimal Simultaneous Multistep Excitations for Aircraft Parameter Estimation," *Journal of Aircraft*, Vol. 54, No. 2, 2017, pp. 747–758. doi:10.2514/1.C033794.

[5] Roeser, M. S., and Fezans, N., "Method for designing multi-input system identification signals using a compact time-frequency representation," *CEAS Aeronautical Journal*, Vol. 12, No. 2, 2021, pp. 291–306. doi:10.1007/s13272-021-00499-6.

[6] Deiler, C., "A Smart Data Approach to Determine an Aircraft Performance Model From an Operational Flight Data Base, AIAA 2023-0797," AIAA SciTech Forum, American Institute of Aeronautics and Astronautics, Inc. (AIAA), National Harbor, MD, USA, 2023. doi:10.2514/6.2023-0797.

[7] Abdelmoula, F., and Scholz, M., "LNAS - A Pilot Assistance System For Low-Noise Approaches With Minimal Fuel Consumption," 31st Congress of the International Council of the Aeronautical Sciences (ICAS), Belo Horizonte, Brazil, 2018. URL https://www.icas.org/ICAS_ARCHIVE/ICAS2018/data/papers/ICAS2018_0096_paper.pdf.

[8] Kühne, C. G., Scholz, M., and Abdelmoula, F., "LNAS - A Pilot Assistance System For Energy-Optimal Approaches Using Existing Aircraft-Infrastructure," *AEGATS 2018*, Advanced Aircraft Efficiency in a Global Air Transport System Conference (AEGATS), Association Aéronautique et Astronautique de France (3AF), Toulouse, France, 2018. URL https://elib.dlr.de/122571.

[9] Gerber, M., Schreiber, Y., Abdelmoula, F., Kühne, C. G., Jager, D., and Wunderli, J.-M., "Energy-optimized approaches: a challenge from the perspectives of pilots and air traffic controllers," *CEAS Aeronautical Journal*, Vol. 13, No. 4, 2022, pp. 1055–1066. doi:10.1007/s13272-022-00607-0.

[10] Burley, C. L., Brooks, T. F., Humphreys, W. M. J., and Rawls, J. W. J., "ANOPP Landing Gear Noise Prediction Comparisons to Model-Scale Data," AIAA, Toronto, Ontario, Canada, 2007. doi:10.2514/6.2007-3459.

[11] Holzäpfel, F., and Schwarz, C. (eds.), *The DLR Project Land-Based and Onboard Wake Systems L-bows*, ISSN: 1434-8454, Deutsche Forschungsanstalt für Luft- und Raumfahrt e. V. (DLR), Cologne, Germany, 2019. DLR-FB2019-16.

[12] Bennett, G. J., Neri, E., and Kennedy, J., "Noise Characterization of a Full-Scale Nose Landing Gear," *Journal of Aircraft*, Vol. 55, No. 6, 2018, pp. 2476–2490. doi:10.2514/1.C034750.

[13] Bertsch, L., Pott-Pollenske, M., Wienke, F., Kurz, J., and Delfs, J., "Retrofit Measures for Aircraft Noise Reduction: Simulation Benchmark and Impact Assessment," *Journal of Aircraft*, Vol. 0, No. 0, 0, pp. 1–16. doi:10.2514/1.C037819.

[14] Zhao, K., Liang, Y., Yue, T., Chen, Z., and Bennett, G. J., "Characterization of the aircraft bay/landing gear coupling noise at low subsonic speeds and its suppression using leading-edge chevron spoiler," *Advances in Mechanical Engineering*, Vol. 11, No. 8, 2019, p. 1687814019871431. doi:10.1177/1687814019871431.

[15] Deiler, C., "Engine thrust model determination and analysis using a large operational flight database," *CEAS Aeronautical Journal*, Vol. 14, No. 1, 2023, pp. 29–45. doi:10.1007/s13272-022-00625-y.

[16] Deiler, C., "Aerodynamic model adjustment for an accurate flight performance representation using a large operational flight data base," *CEAS Aeronautical Journal*, Vol. 14, No. 2, 2023, pp. 527–538. doi:10.1007/s13272-023-00659-w.

[17] "Flight dynamics – Concepts, quantities and symbols – Part 1: Aircraft motion relative to the air," Standard, International Organization for Standardization (ISO), Geneva, Switzerland, Apr. 1988. ISO 1151-1:1988.

[18] AIAA (ed.), *Recommended Practice for Atmospheric and Space Flight Vehicle Coordinate Systems*, American National Standards Institute - American Institute of Aeronautics and Astronautics, 1992.

[19] Raab, C., "Rapid Aerodynamic Parameter Identification on a Large Transport Aircraft," AIAA Atmospheric Flight Mechanics Conference at SciTech, American Institute of Aeronautics and Astronautics, Inc., National Harbor, Maryland, USA, 2014. doi:10.2514/6.2014-0730.

[20] Moennich, W., "Ein 2-Punkt-Aerodynamikmodell für die Identifizierung," Symposium 'Systemidentifizierung in der Fahrzeugdynamik', Paper No 3.1 in DFVLR Mitteilung 87-22 (in German), 1987.

[21] Fischenberg, D., and Jategaonkar, R. V., "Identification of Aircraft Stall Behavior from Flight Test Data," RTO Systems Concepts and Integration Panel (SCI) Symposium, Paper No 17, NATO Research and Technology Organisation, Madrid, Spain, 1998.

[22] Jategaonkar, R., *ldentification of the Aerodynamic Model of the DLR Research Aircraft ATTAS from Flight Test Data*, DLR-FB 90-40, Deutsche Forschungsanstalt für Luft- und Raumfahrt e. V. (DLR), Cologne, Germany, 1990.

[23] Fischenberg, D., "Identification of an unsteady aerodynamic stall model from flight test data," AIAA Atmospheric Flight Mechanics Conference, American Institute of Aeronautics and Astronautics, Inc. (AIAA), Baltimore, Maryland, USA, 1995, pp. 138–146. doi:10.2514/6.1995-3438.

[24] Deiler, C., "Engine Thrust Model Determination from Large Operational Flight Data Base," 6th CEAS Conference on Guidance, Navigation and Control (EuroGNC), Council of European Aerospace Societies (CEAS), Berlin, Germany, 2022. URL https://eurognc.ceas.org/archive/EuroGNC2022/pdf/CEAS-GNC-2022-013.pdf.